The bootstrap current in small rotating magnetic islands

A. Bergmann, E. Poli

Max-Planck-Institut für Plasmaphysik, IPP–EURATOM Association,

D-85748 Garching bei München, Germany

A. G. Peeters

Centre for Fusion, Space and Astrophysics, Department of Physics,

University of Warwick, Coventry CV4 7AL, UK

Abstract

The bootstrap current in small magnetic islands of neoclassical tearing modes is studied with guiding center particle simulations including pitch angle scattering. A model for a rotating island and its electric field is used and a new approximation to the electric potential in small islands is derived. Islands with sizes of the order of the ion banana orbit width are studied by means of a two-step model which allows to treat both ions and electrons kinetically. The bootstrap current in such small islands is found to depend strongly on the direction of rotation of the island. The bootstrap current in small islands rotating in the ion diamagnetic direction is strongly diminished, similarly to what happens in big islands. In small islands rotating in the electron diamagnetic direction, on the contrary, the bootstrap current is almost completely preserved, implying a reduced neoclassical drive of the island growth.

I. INTRODUCTION

Neoclassical tearing modes play an important role in present large tokamak experiments, and the planned international experiment ITER, since they set a limit to the achievable pressure in long-pulse operation with high confinement [1]. A tearing mode occurs when a magnetic perturbation creates by field line reconnection a small unstable helical island structure in the plasma. In a tokamak, the flattening of the pressure profile due to the fast transport along the field lines inside a sufficiently big island causes a loss of the bootstrap current at the position of the island. This loss corresponds to a perturbed current in the opposite direction that can drive the mode unstable even when the unperturbed current profile would be stabilizing [2, 3]. In this case the mode is called a neoclassical tearing mode (NTM).

It is generally assumed that in small islands, due to the incomplete flattening of the density and temperature profiles, the bootstrap current is not entirely lost. The incomplete flattening of the pressure profile in a small island is due, on the one hand, to the fact that the parallel transport is indeed very high but finite. This implies that there exists always a layer around the island separatrix where the perpendicular transport across the separatrix competes with the parallel transport. Profile flattening is strongly reduced when the island width is of the order of the width of this layer. For the temperature profile, e.g., the critical size is about $(\chi_\perp/\chi_\parallel)^{1/4} (rR_0)^{1/2}$ [4], where $\chi_\perp$ and $\chi_\parallel$ are the perpendicular and parallel heat conductivities, respectively. A second reason for the incomplete disappearance of the bootstrap current is the effect of the finite ion banana orbit width, which is important when the island width is comparable or smaller than the typical ion orbit width. Previous kinetic investigations [5, 6] of the bootstrap current in small static islands have shown that the ion component of the bootstrap current is entirely restored when the island width falls below the thermal ion banana width.

In this work, we study the effect of the finite ion orbit width on the bootstrap current in small islands. In addition to the model used in Refs. 5, 6, we take into account the rotation of the island and the corresponding electric field. As is well known (cf. section III), in the presence of a radial electric field E_r, the neoclassical damping of poloidal rotation leads to a contribution to the parallel flow of both ions and electrons proportional to the ratio between E_r and the poloidal magnetic field B_p [7]. In general, these flows do not lead to an electrical current. In the case of a small island, however, the response to the island electric field (which has large variations across the island separatrix) can be different for

ions and electrons because of the different width of their orbits, so that a finite parallel current can be generated. Since the direction of the E_r/B_p flow is related to the direction of the island rotation with respect to the surrounding plasma, the contribution of such a current to the island dynamics can be stabilizing or destabilizing depending on the sign of the island rotation frequency. Here, we study the response of both ions and electrons to islands rotating in either direction, treating the island width and the rotation frequency as input parameters. The surface-averaged parallel current, the changes of the density and temperature profiles and the plasma flow are determined by means of guiding center particle simulations. Ions and electrons are treated kinetically, including ion-ion, electron-electron and electron-ion collisions, according to the two-step model presented in section II.

II.   THE SIMULATION MODEL

A.   Perturbed equilibrium with rotating island

The magnetic field used in the numerical simulations consists of a simple equilibrium field with concentric circular flux surfaces and a perturbation that creates a rotating island with a single helicity. The toroidal and poloidal components of the equilibrium magnetic field are

$$B_t = \frac{B_0}{1 + \varepsilon \cos \vartheta}, \qquad B_p = \frac{\varepsilon B_t}{q\sqrt{1 - \varepsilon^2}}. \tag{1}$$

This field is expressed in Boozer coordinates ψ, θ, ζ as

$$\boldsymbol{B} = \nabla \zeta \times \nabla \psi + q(\psi) \nabla \psi \times \nabla \theta. \tag{2}$$

where ψ is the poloidal flux, q is the safety factor, and θ and ζ are poloidal and toroidal angles. The Boozer angle θ is related to the angle ϑ appearing in equation (1) by $\tan(\theta/2) = \sqrt{(1-\varepsilon)/(1+\varepsilon)} \tan(\vartheta/2)$ [6]. We assume $q = 1 + q'\psi$ with a constant q'. From the definition of the toroidal flux (per radian),

$$2\pi\psi_t = \int B_t R_0^2 \varepsilon d\varepsilon d\vartheta, \tag{3}$$

and $\psi_t = \int q(\psi)d\psi$ we obtain the poloidal flux ψ as a function of the inverse aspect ratio ε,

$$\psi + q'\psi^2/2 = R_0^2 B_0 (1 - \sqrt{1 - \varepsilon^2}). \tag{4}$$

A perturbation of the vector potential

$$\delta A_\parallel = -\hat{\alpha} \cos(\xi) R_0 B, \quad \xi = m\theta - n\zeta - \omega t, \tag{5}$$

with mode numbers m and n, mode frequency ω, $B = \sqrt{B_t^2 + B_p^2}$ and a constant $\hat{\alpha}$ is assumed. This leads to the poloidal flux perturbation

$$\delta\psi = \hat{\alpha} R_0 R B_t \cos\xi = \hat{\psi} \cos\xi \tag{6}$$

that creates, near the flux surface with $q = q_s = m/n$, a rotating helical island of size $w_\psi = \sqrt{4\hat{\psi}q_s/q_s'}$ (half of the poloidal flux difference across the island) and half-width $w_{\text{isld}} \approx (dr/d\psi)w_\psi$. The index s indicates the resonant surface, the prime denotes the derivative with respect to the poloidal flux ψ and ξ is a helical angle. The perturbed poloidal flux is not suited as a label for the perturbed flux surfaces inside and near the island. Employing both ψ and ψ_t we can define a helical flux as $\Psi_{\text{hel}} = \psi - \psi_t/q_s + \hat{\psi}\cos\xi$, which is constant on the perturbed flux surfaces. In the following we use, as an alternative to ψ, θ, ζ, a normalized helical flux obtained from a second-order expansion of ψ_t around ψ_s,

$$\Omega = 2(\psi - \psi_s)^2/w_\psi^2 - \cos\xi \tag{7}$$

together with ξ and θ. $\Omega = 1$ defines the island separatrix and $\Omega = -1$ is the minimum value of Ω attained at the O point ($\xi = 0, \psi = \psi_s$) of the island. For the time-dependent electric potential of the rotating island we use two different analytic approximations. First we take the well-known expression [8, 9]

$$\Phi = \frac{q\omega}{m}\left\{(\psi - \psi_s) \pm \frac{w_\psi}{\sqrt{2}}(\sqrt{\Omega} - 1)\Theta(\Omega - 1)\right\}, \tag{8}$$

which was derived assuming $E_\parallel = -\partial A_\parallel/\partial t - \nabla_\parallel\Phi = 0$. The positive sign holds for $\psi < \psi_s$ and Θ is defined as $\Theta(x) = 1$ for $x \geq 0$ and $\Theta(x) = 0$ for $x < 0$. The first part of Φ is constant on the unperturbed flux surfaces and the corresponding part of the electric field is $E_r = -(q\omega/m)\nabla\psi \approx -(q\omega/m)RB_p$. It causes the plasma inside the island to co-rotate with the island, since $(\boldsymbol{E} \times \boldsymbol{B})_\theta/r = \omega/m$ is the poloidal rotation frequency of the island. The second part of Φ reduces the electric field $-\nabla\Phi$ outside the island, such that it vanishes far away from the island, where the plasma is assumed to be at rest. The expression for Φ in equation (8) is valid for big islands, but we shall show that in small islands the potential can be very different, depending on the rotation frequency. A second expression for the potential, valid in small islands, is derived in section IV.

B. Two step δf model

The bootstrap current is a flux surface averaged parallel current which is driven by radial gradients of density or temperature. A kinetic description of the bootstrap current

generation is obtained from the drift kinetic equation

$$\frac{df}{dt} = \frac{\partial f}{\partial t} + \boldsymbol{v} \cdot \nabla f + \left(\frac{e\boldsymbol{v} \cdot \boldsymbol{E}}{mv_\parallel} - \frac{\mu \nabla_\parallel B}{m} \right) \frac{\partial f}{\partial v_\parallel} = C(f) \tag{9}$$

for the distribution function $f(\boldsymbol{r}, v_\parallel, \mu)$ of the guiding centers. Here, $\boldsymbol{v} = v_\parallel \boldsymbol{b} + \boldsymbol{v}_d$ is the guiding center velocity with parallel component $v_\parallel$, $\boldsymbol{b} = \boldsymbol{B}/B$, and drift velocity $\boldsymbol{v}_d = \boldsymbol{B} \times (mv_\parallel^2(\boldsymbol{b} \cdot \nabla)\boldsymbol{b} + \mu \nabla B + e\nabla\Phi)/eB^2$, $\mu = mv_\perp^2/2B$ is the magnetic moment, $\boldsymbol{E} = -\boldsymbol{b}\,dA_\parallel/dt - \nabla\Phi$ is the electric field, and $C(f)$ is the collision operator. We have to solve the kinetic equations for ions and for electrons. Since we assume a given magnetic field with prescribed perturbation and electric field, the only coupling between the ion and electron equations is via the collision operator. For the ions we can neglect collisions with electrons, because their effect on the ion momentum is very small. This makes it possible to compute the electric current in two steps: First the equations for the ions are solved with $C(f_i) = C_{ii}(f_i)$ to obtain the distribution function f_i. In the second step the equations for the electrons are solved, where the collision operator, $C(f_e) = C_{ee}(f_e) + C_{ei}(f_e, f_i)$, depends on f_i, because here it is important to include the friction between electrons and ions. With this procedure there is no need to follow the electrons for several ion collision times, but several electron collision times are sufficient. The procedure was successfully tested with a different code, but with the same collision model [10].

We apply the δf method, i.e. the distribution function is split into two parts, $f = f_0 + \delta f$, and only the part δf is represented by marker particles, which trace the guiding center orbits. f_0 is chosen suitably with $|\delta f| \ll f_0$ in order to make efficient use of the marker particles. For the ions we choose a local Maxwellian on the unperturbed flux surfaces,

$$f_{i0} = \frac{n_{i0}(\psi)}{(2\pi T_{i0}(\psi)/m_i)^{3/2}} \exp\left\{ -\frac{mv^2/2}{T_{i0}(\psi)} \right\}. \tag{10}$$

Here, m_i is the ion mass and $n_{i0}(\psi)$ and $T_{i0}(\psi)$ are the initial radial profiles of ion density and temperature. This choice reduces the collision operator to $C_{ii}(\delta f_i, f_{i0})$, since $C(f_{i0}) = 0$ holds. For the electrons we choose f_{e0} as a Maxwellian centered at the ion flow velocity $u_{i\parallel}$,

$$f_{e0} = \frac{n_{e0}(x)}{(2\pi T_{e0}(x)/m_e)^{3/2}} \exp\left\{ -\frac{m_e(v_\parallel - u_{i\parallel}(x))^2/2 + \mu B}{T_{e0}(x)} \right\}, \tag{11}$$

and in the coefficients of $C_{ei}(f_e, f_i)$ we approximate f_i by a similar Maxwellian (the exact form of f_i is not important, since the ion velocities are much smaller than the electron velocities),

$$f_{iM} = \frac{n_i(x)}{(2\pi T_i(x)/m_i)^{3/2}} \exp\left\{ -\frac{m_i(v_\parallel - u_{i\parallel}(x))^2/2 + \mu B}{T_i(x)} \right\}. \tag{12}$$

In these expressions, $n_i(x)$ and $T_i(x)$ are the radial ion density and temperature profiles obtained from the ion distribution function determined in the first step, and we take $n_{e0} = n_i$. The variable x is either ψ or Ω depending on what choice fits better the solution of the ion equation. This choice of f_{e0} and f_i reduces the electron collision operator to

$$C(\delta f_e) = C_{ee}(\delta f_e, f_{e0}) + C_{ei}(\delta f_e, f_{iM}), \tag{13}$$

which is applied in the frame of reference moving with the ion velocity. The distribution function f_{e0} in equation (11) gives a finite contribution to the parallel electric current that just cancels the ion current $en_i u_{i\parallel}$. Hence, the bootstrap current is obtained directly from an the integral over δf_e. With these choices for f_{i0} and f_{e0} we arrive at the following equations

$$\frac{d\delta f}{dt} = C(\delta f) - \frac{df_0}{dt}. \tag{14}$$

We use the Hamiltonian guiding center particle code HAGIS [11] which contains a Monte Carlo procedure for pitch-angle scattering [12]. The Hamiltonian guiding center equations for the marker particles are consistently obtained from a Lagrangian. They are expressed in the Boozer coordinates ψ, θ, ζ and the velocity space coordinates $\rho_\parallel = mv_\parallel/eB$ and μ and solved by a Runge-Kutta method with adaptive time steps. Associated with each particle is a phase space element and the contribution of the particle to δf, the product of which is the particle's weight. The sources for this weight are the terms on the right-hand side in equation (14). The effect of collisions is included as follows: The particles move collisionless for the length of a collision of time step and then the change of their velocities and weights by collisions is determined as explained in the next subsection.

Without collisions the distribution function f would be constant along the particle orbit as expressed by equation (14). Hence, between collisions we can compute δf as the difference between the value f_j of the total distribution function on the particle orbit and the value of f_0 at the current position of the particle in phase space [13]. For the jth particle we get

$$\delta f_j(t) = f_j - f_0(\boldsymbol{r}_j(t), \boldsymbol{v}_j(t)) \tag{15a}$$

$$f_j(0) = f_0(\boldsymbol{r}_j(0), \boldsymbol{v}_j(0)). \tag{15b}$$

Between collisions f_j is constant, but when collisions occur, their contributions to the particle weights have to be added to δf_j. This is achieved by changing f_j in the collision procedure.

C. Monte Carlo procedure for pitch angle scattering

The collision operator for pitch-angle Coulomb scattering is applied. For scattering of particles α by particles β with a Maxwellian distribution it reads

$$C_{\alpha\beta}(f_\alpha, f_{\beta M}) = \hat{\nu}_{\alpha\beta}(v) \frac{1}{2} \frac{\partial}{\partial\lambda} (1 - \lambda^2) \frac{\partial f_\alpha}{\partial\lambda}, \tag{16}$$

where $\lambda = v_\parallel/v$ is the cosine of the pitch angle, and $\hat{\nu}_{\alpha\beta}(v)$ is the velocity-dependent collision frequency. It is obtained from the pitch angle part of the Landau-Fokker-Planck collision term [equation (6.40) in Ref. 7],

$$\hat{\nu}_{\alpha\beta}(v) = \nu_{0\alpha\beta} \left(\frac{v_{\text{th}\alpha}}{v}\right)^3 G\left(\frac{v}{v_{\text{th}\beta}}\right), \tag{17a}$$

$$G(x) = \left(1 - \frac{1}{2x^2}\right) \text{erf}(x) + \frac{\exp(-x^2)}{x\sqrt{\pi}}. \tag{17b}$$

The quantity $\nu_{0\alpha\beta} = n_\beta Z_\alpha^2 Z_\beta^2 e^4 \ln \Lambda_{\alpha\beta}/(4\pi\epsilon_0^2 m_\alpha^2 v_{\text{th}\alpha}^3)$ is related to the usual collision frequencies $(\nu_{ii}, \nu_{ee}, \nu_{ei})$ by $\nu_{\alpha\beta} = 4\nu_{0\alpha\beta}/3\sqrt{2\pi}$. The thermal velocities are defined as $v_{\text{th}\alpha} = \sqrt{2T_\alpha/m_\alpha}$ and $v_{\text{th}\beta} = \sqrt{2T_\beta/m_\beta}$. For the electron-ion collisions $G(x)$ is replaced by the asymptotic value $G = 1$ for $x = v_e/v_{\text{thi}} \gg 1$. The changes of $v_\parallel$ and $v_\perp$ during a collision time step Δt_c are computed with (pseudo) random numbers η fulfilling $\langle\eta\rangle = 0$ and $\langle\eta^2\rangle = 1$ as follows

$$\delta v_\parallel = -\hat{\nu} v_\parallel \Delta t_c + \eta v_\perp \sqrt{\hat{\nu}\Delta t_c}, \tag{18a}$$

$$\delta v_\perp^2 = -(2v_\parallel + \delta v_\parallel)\delta v_\parallel. \tag{18b}$$

The pitch angle scattering does not conserve the particle momentum, but we achieve momentum conservation in a second step by adding a term proportional to $\hat{\nu} v_\parallel f_M$ [14, 15] to δf, i.e. we change the values f_j in equation (15a) by

$$\delta f_{\text{corr.}} = -\hat{\nu}(v) v_\parallel f_M \Delta p_\parallel \; / \int \hat{\nu}(v) m v_\parallel^2 f_M d^3 v, \tag{19}$$

where $\Delta p_\parallel = \int m \delta v_\parallel \delta f d^3 v$ is the momentum change in the Monte Carlo step. In the numerical simulation it is not possible to compute $\delta f_{\text{corr.}}$ at each point in real space, since a minimum number of marker particles is needed for representing the velocity space in the integral in equation (19). Therefore the correction is done within volume elements of finite size that are constructed as follows. The plasma volume is divided into thin shells between helical flux surfaces with a closer spacing near the island for sufficient resolution. These
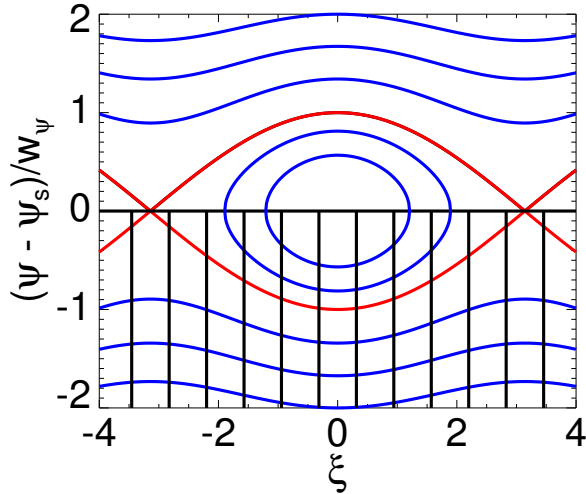
7

FIG. 1: Lines of constant helical flux in the ξ-ψ plane (schematic). In the lower half of the graph the grid cells for computing ξ-dependent averages and integrals for the collision operator are indicated. w_ψ is the island half-width.

volumes between flux surfaces are then subdivided further into smaller cells to avoid a possible spurious momentum transfer along the helical angle coordinate ξ. The range of ξ from $-\pi$ to π is divided into 10 bins as indicated in the lower half of Fig. 1. The Monte Carlo procedure described above was successfully tested in Refs. 10, 12, 16.

D. Flux surface averages

The flux surface averages are approximated by volume averages within a thin shell between two helical flux surfaces,

$$\left\langle \int A \, \delta f \, d^3v \right\rangle \approx \int_{\Omega-\delta\Omega}^{\Omega+\delta\Omega} A \, \delta f \, d\Gamma \, / \int_{\Omega-\delta\Omega}^{\Omega+\delta\Omega} \mathcal{J} d\Omega d\xi d\theta, \tag{20}$$

where $\mathcal{J}$ is the Jacobian and $d\Gamma = d^3v \, \mathcal{J} d\Omega d\xi d\theta$ is the phase space volume element. The integral in the numerator of equation (20) is replaced by a sum over the contributions of the marker particles,

$$\sum_{\Omega-\delta\Omega \leq \Omega_j \leq \Omega+\delta\Omega} A_j \, \delta f_j \, \Delta\Gamma_j, \tag{21}$$

where $\Delta\Gamma_j$ is the phase space volume associated with the jth marker, and δf_j the marker's contribution to δf. The integral in the denominator is computed numerically directly from

$\mathcal{J}$. Whenever the dependence of some variable on the helical angle ξ is to be resolved, the averages are computed for the grid cells indicated in lower half of Fig. 1.

III. THE SMALL-ISLAND EFFECT

The island of a neoclassical tearing mode is normally rotating with respect to the surrounding plasma and a radial electric field is present inside the island that acts to force the plasma to co-rotate with the island. (We consider the frame of reference in which the plasma far from the island is at rest.) Since the trapped particles, on average, cannot follow the poloidal $\boldsymbol{E} \times \boldsymbol{B}$ drift and by collisions the poloidal rotation of the passing particles is also damped, a contribution $u_\parallel = \langle E_r/B_p \rangle$ to the parallel flow velocity arises [7], where the brackets indicate the flux surface average. In a big island the parallel flow velocities of ions and electrons are equal and thus do not contribute to the electric current. When, however, the island width is of order of the ion banana orbit width, this is not the case, and a finite electric current arises. This effect can best be seen in the artificial case of a rotating island in plasma with constant background density and temperatures (equal for ions and electrons) such that no unperturbed current exists. We demonstrate the creation of this current with numerical results for a small island with $w = 0.6$. Here and in the following we denote by w the ratio of the island width and the ion orbit width,

$$w = w_{\text{isld}}/w_{\text{ion}} \tag{22}$$

with $w_{\text{ion}} = \sqrt{\varepsilon}\rho_{ip}$ and $\rho_{ip} = mv_{\text{th}i}/eB_p$. The following parameters have been used for the calculations: $n_0 = 10^{20}\text{m}^{-3}$, $T_0 = 1000$ eV, $\omega = 13000s^{-1}$, $B_0 = 2$T, $R_0 = 2$m; the safety factor q varies radially between 1 and 3, and the island is located at a flux surface with $q = m/n = 3/2$ and inverse aspect ratio $\varepsilon = 0.22$; the collision frequency is set to a value corresponding to $\nu^* = \nu q R/\epsilon^{3/2} v_{\text{th}} = 0.02$ at the location of the island.

The parallel ion flow velocity in steady state after 8 collision times is shown in Fig. 2(a). In the island the flow velocity is much smaller than the neoclassical velocity $\langle E_r/B_p \rangle$, because the ions do not feel the strong electric field all along their orbits, but only inside the island. In addition, due to the finite orbit width a finite ion flow exists outside the island, although the electric field is very small. The electron velocity, on the contrary, is close to $\langle E_r/B_p \rangle$ due to the small electron orbit width, as is shown in Fig. 2(b), when electron-ion collisions are switched off. This mismatch of the flows results in a finite electric current in the island of the order of $\langle -enE_r/B_p \rangle$, which is reduced to a smaller value, when the friction due to
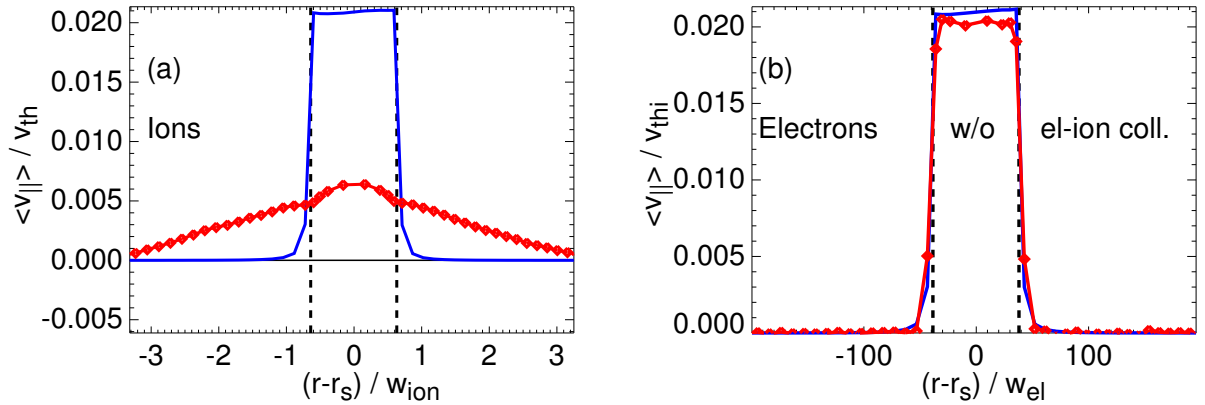
9

FIG. 2: (a) Parallel ion flow velocity (red symbols), and (b) parallel electron flow velocity (red symbols) from a simulation without e-i collisions versus the radius through the O point of a small rotating island ($w = 0.6$). Also shown by solid blue lines is $\langle E_r / B_p \rangle$.
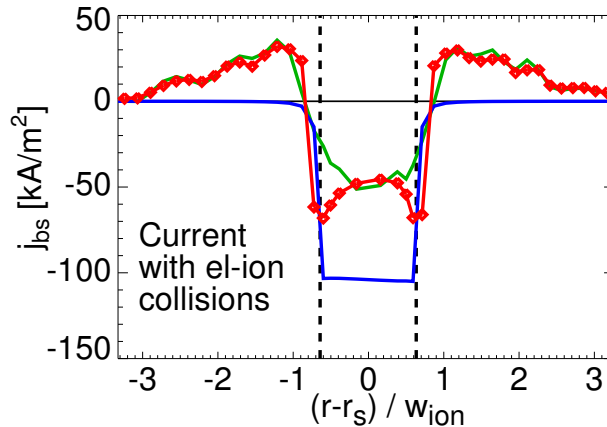

FIG. 3: Parallel electric current (red symbols) in the island of Fig. 2. Also shown is the current $\langle -enE_r / B_p \rangle$ (solid blue line) and the bootstrap current computed with the perturbed density gradient (green/grey line).

collisions between electrons and ions is included. This is shown in Fig. 3, where the electric current from a simulation with electron-ion collisions is depicted.

The finite electric current goes along with a small density perturbation of order $-e\Phi/T$ shown in Fig. 4, which creates a finite density gradient in the island and outside the island near the separatrix. We find that the values of the ion flow and the bootstrap current obtained from the usual neoclassical theory [7, 17] with the *perturbed* density gradient match
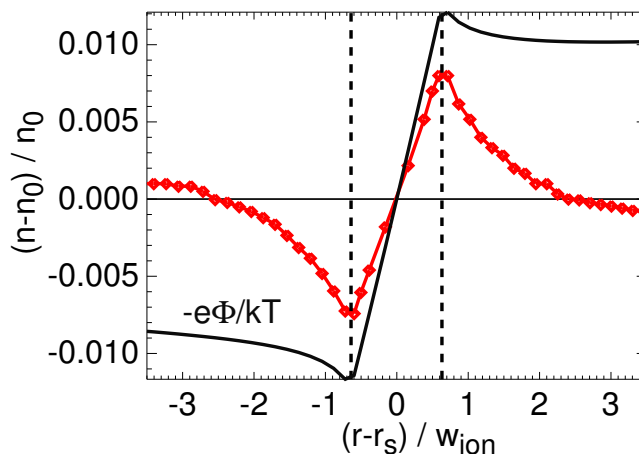
10

FIG. 4: Density perturbation (symbols) in the island in Fig. 2 compared to $-e\Phi/T$ (solid line) for an island rotating in the ion diamagnetic direction.

well the numerical results, except close to the separatrix. This might be surprising since the island is smaller than the ion banana orbit width, but, on the other hand, the density variation is only a percent or two over the island width, hence the gradient length $n/(dn/dr)$ is much larger than the island width. Near the separatrix the strong change of the gradient evidently has an effect. The density perturbation and the electric current have the opposite sign when the island is rotating in the opposite direction, since the potential is proportional to ω. In the normal case of negative density and temperature gradients the additional small-island current has the same direction as the unperturbed bootstrap current, when the island rotates in the direction of the electron diamagnetic drift, and it has the opposite direction in the case of rotation in the ion diamagnetic drift direction.

IV. RESULTS OF THE SIMULATIONS

A. Results with electric potential like in big islands

In the simulations, the mode frequency ω is a free parameter, while in the experiment it depends on the density and temperature gradients of the unperturbed plasma. From analytic models for neoclassical tearing modes values $\omega = \omega_* (1 + \kappa\eta)$ near either of the diamagnetic frequencies,

$$\omega_{*e} = -\frac{mT_e}{qen_0}\frac{dn_0}{d\psi}, \qquad \omega_{*i} = \frac{mT_i}{qen_0}\frac{dn_0}{d\psi}, \tag{23}$$

11

are obtained [18], where $\eta = nT'/Tn'$ is the ratio of the logarithmic gradients and κ is a factor smaller than unity (since ω is m times the island rotation frequency, the diamagnetic frequencies are multiplied by m here). For such frequencies the current of order $\langle enE_r/B_p \rangle$ found in the previous section is of similar size as the unperturbed bootstrap current: $\langle enE_r/B_p \rangle \approx en(q\omega_*/mB_p)d\psi/dr \approx (T/B_p)dn/dr$. Therefore, the bootstrap current in small islands can differ considerably from that in big islands. The partial preservation of the ion bootstrap current which we found in small non-rotating islands [6] is enhanced or diminished depending on the direction of rotation.

We performed simulations for small islands with finite density and temperature gradients in the unperturbed plasma. The density profile is chosen as $n = n_0 \exp\{-\gamma\psi/\psi(a)\}$ with $\gamma = 1$ or $\gamma = 0.5$ and $n_0 = 10^{20}\mathrm{m}^{-3}$ (a is the minor radius, with $a/R_0 = 0.333$). The temperature has the same profile, $T = T_0 \exp\{-\gamma\psi/\psi(a)\}$, where T_0 is varied (500eV – 2000eV) together with the magnetic field B_0 (2T – 6T) and the perturbation strength $\hat{\alpha}$ ($2 \cdot 10^{-6} - 4 \cdot 10^{-5}$) in order to get the desired ratio $w = w_{\mathrm{isld}}/w_{\mathrm{ion}}$ while keeping the island size small compared to the minor radius. Again, the safety factor q varies radially between 1 and 3, with $q = m/n = 3/2$ and $\varepsilon = 0.22$ at the location of the island. The collision frequency is scaled by a constant factor in order to obtain $\nu^* = \nu q R/\epsilon^{3/2} v_{\mathrm{th}} \approx 0.02$ at the location of the island, such that the plasma is in the banana regime.

In Fig. 5, the bootstrap current (surface averaged parallel electric current) in the island region is shown for different values of w. In the left column the results for islands rotating at the ion diamagnetic frequency are depicted, and in the right column the results for islands rotating at the electron diamagnetic frequency. In the case $\omega = \omega_{*i}$, the small-island current is opposite to the unperturbed bootstrap current and we see that only a small fraction the unperturbed bootstrap current remains present in the island. That implies that almost the full bootstrap current drive for the NTM remains present in this case. With rotation at $\omega = \omega_{*e}$, however, the current due to the small-island effect is in the same direction as the bootstrap current, and a large fraction of the unperturbed bootstrap current is preserved in the island. In this case the drive of the mode due to the bootstrap current is strongly reduced in small islands.

In Fig. 5 also the bootstrap current values obtained from the neoclassical theory [17] with the perturbed density and temperature gradients are shown. They match well with the numerical results, except near the separatrix, particularly in the case $\omega = \omega_{*e}$. Looking at the perturbed density and temperature profiles in Figs. 6 and 7(a), we notice that in this case the flattening of the electron density and temperature in the island produces enhanced
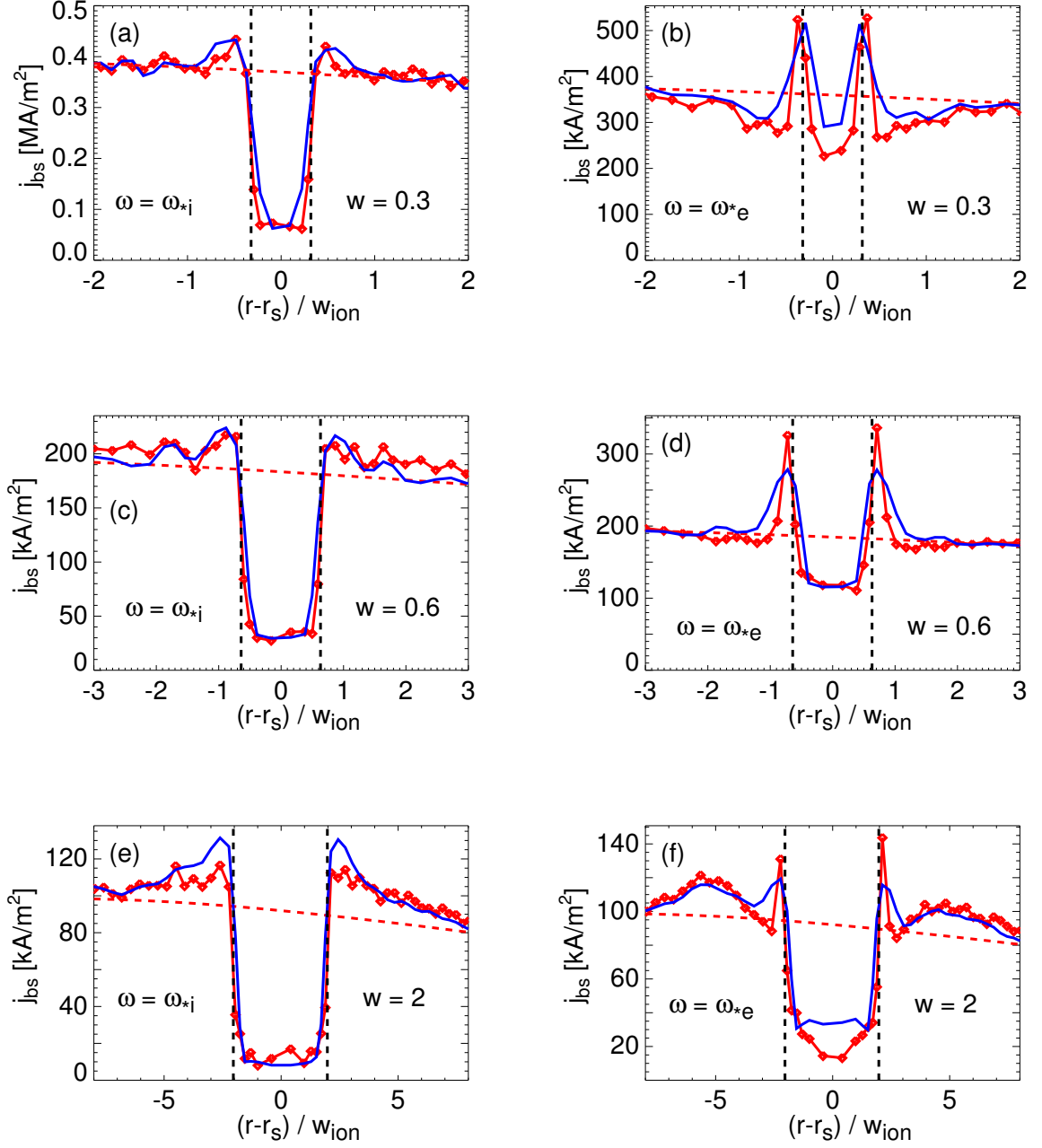
12

FIG. 5: Bootstrap current from simulations (red symbols) in islands rotating at the ion diamagnetic frequency (a,c,e) or the electron diamagnetic frequency(b,d,f), $w = w_{isld}/w_{ion}$ is the normalized island width. Also shown is the neoclassical value computed with the perturbed gradients (solid blue line) and the unperturbed current (oblique dashed line). Vertical dashed lines indicate the position of the island.
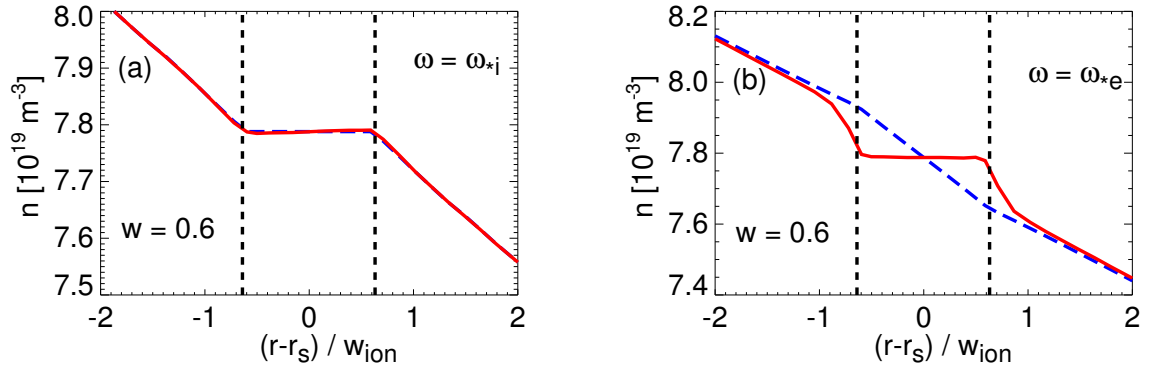
13

FIG. 6: Profiles of electron density (red solid) and ion density (blue dashed) across small islands ($w = 0.6$) rotating at ion diamagnetic frequency (a) or electron diamagnetic frequency (b). Vertical dashed lines indicate the position of the island.
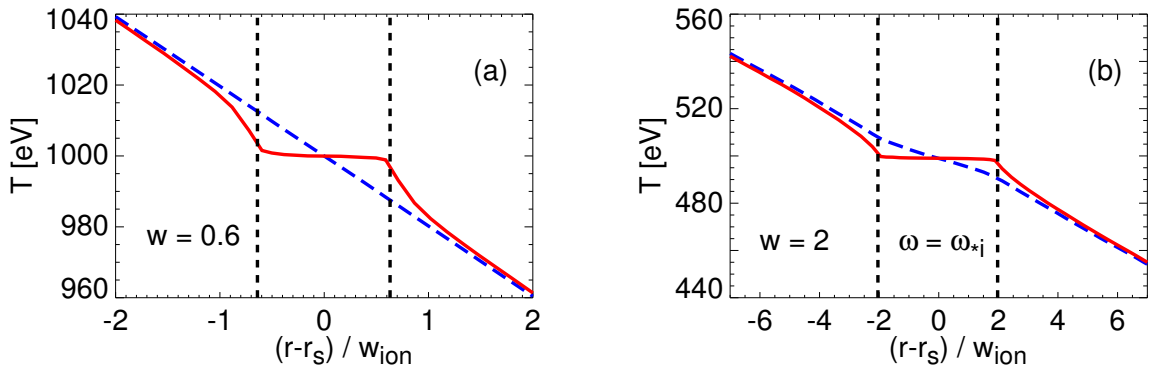

FIG. 7: Electron (red solid) and ion (blue dashed) temperature profiles in a small island (a) with $w = 0.6$ and a bigger island (b) with $w = 2$. Vertical dashed lines indicate the position of the island.

gradients just outside the island, but neither the ion density nor the ion temperature are flattened. The ion temperature profile is unchanged when the island width is smaller than the orbit width. (In the simulations, the finite collisional heat transport tends to flatten a little the temperature profile on a scale much larger than the island width, because there is no heat source. This is not caused by the island and occurs even without the presence of an island.) In islands rotating at the electron diamagnetic frequency the ion density is even steeper than the unperturbed density. This means that quasi neutrality is violated in
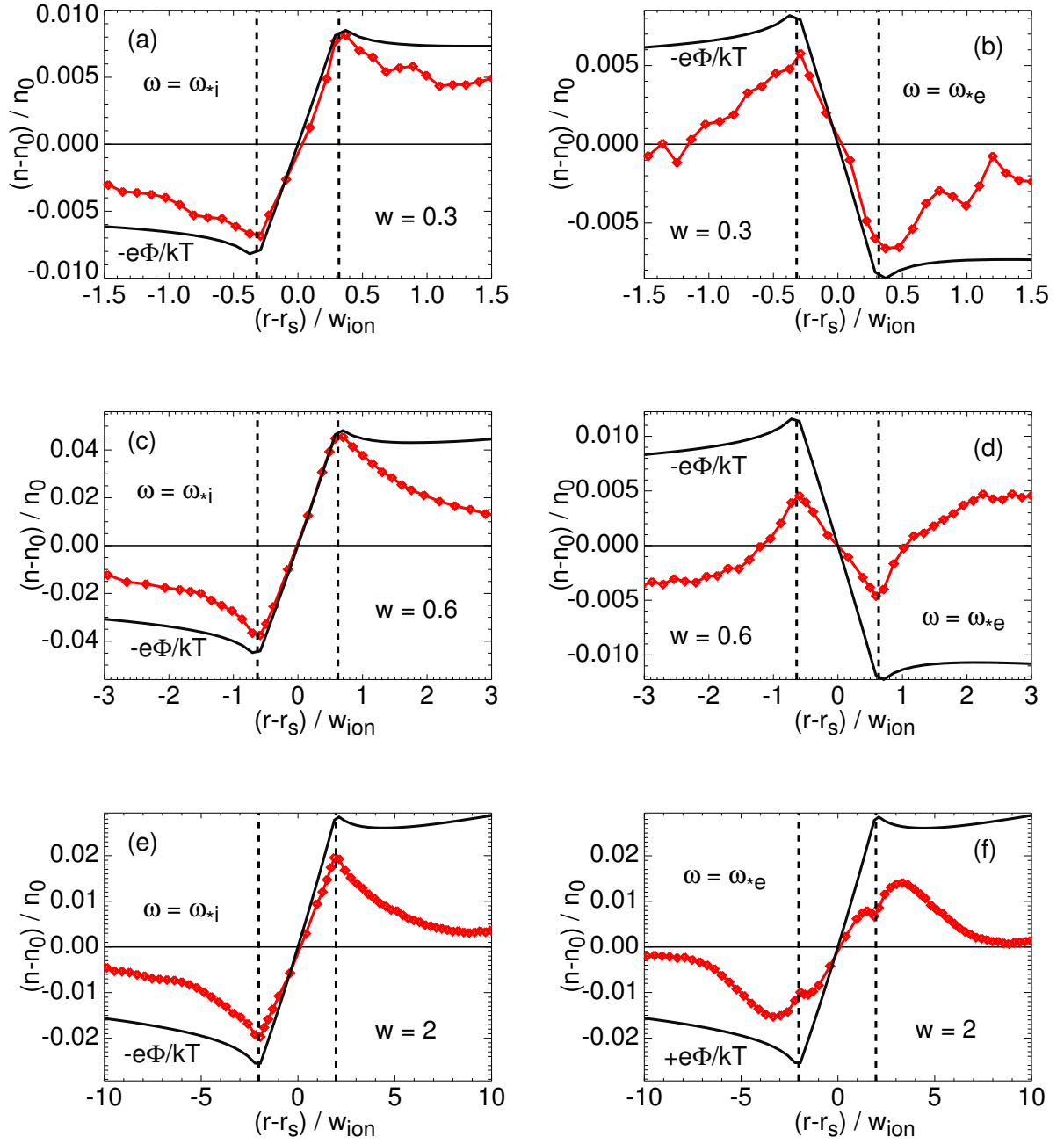
FIG. 8: Density perturbations, $(n-n_0)/n_0$, (red symbols) in islands rotating at the ion diamagnetic frequency (a,c,e) or at the electron diamagnetic frequency (b,d,f). Also shown are $-e\Phi/T_i$ or $+e\Phi/T_i$ (solid black lines), $w = w_{\text{isld}}/w_{\text{ion}}$.

15

this case which makes it necessary to consider a modification of the electric potential which is the subject of Sec. IV B. In the case $\omega = \omega_{*i}$, the ion and electron densities are both flattened in the island and quasi neutrality is preserved. In this case the residual bootstrap current in the island is due to the ion temperature gradient. The ion temperature gradient in the island starts to decrease a little at $w = 2$ as shown in Fig. 7(b) and almost vanishes at $w = 10$.

Looking at the normalized ion density perturbations shown in Fig. 8, we can see how the the plasma reacts differently to the rotating island and its electric field depending on the direction of rotation. In islands rotating at the ion diamagnetic frequency the ion density perturbation is always close to $-e\Phi/T_i$, which corresponds to a flattening of the ion density in Fig. 6 when the potential is given by equation (8). In the case $\omega = \omega_{*e}$ the ion density perturbation varies from $+e\Phi/T_i$ in big islands (not shown here, but this corresponds to flattening) to $-e\Phi/T_i$ in small islands, which corresponds to the steepening seen in Fig. 6.

The combined results of many simulations are shown in Fig. 9, where the fraction of the unperturbed bootstrap current that is preserved in small islands is plotted versus the island width. The difference between the bootstrap current values at $\omega = \omega_{*e}$ and at $\omega = \omega_{*i}$ increases with decreasing island size, but even in islands rotating at the electron diamagnetic frequency the bootstrap current is not entirely preserved. In the simulations there is a finite electron temperature gradient in the unperturbed plasma and the electron temperature profile is flattened. The resulting loss of the contribution due to the electron temperature gradient sets an upper limit to the bootstrap current. For $\omega = \omega_{*i}$ there is a lower limit to the bootstrap current in a small island set by the current driven by the (unchanged) ion temperature gradient. The absolute values of these limits depend on the values of the density and temperature gradients in the unperturbed plasma, and on the neoclassical parameters such as collisionality and trapped particle fraction (in the simulations: $\nu^* \approx 0.02$, $f_t \approx 0.6$ at the position of the island and $\eta = 1$).

B. Results with modified electric potential

The violation of quasi neutrality in the case $\omega \approx \omega_{*e}$ indicates that in such islands the electric field must be different from that derived from the potential in equation (8), which is valid for big islands. In small islands the electric potential is a more complex function of Ω and ξ and waves can be excited by the island [19]. We can get an estimate for the potential as follows: In view of the results presented above, the ion density in small islands
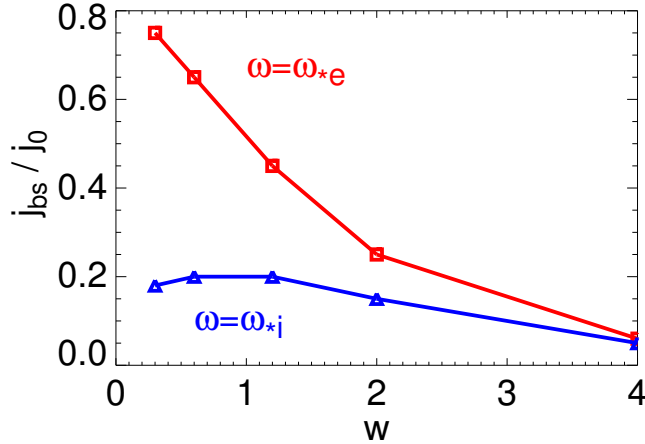
16

FIG. 9: Bootstrap current in the island normalized to the unperturbed current versus normalized island width $w = w_{\mathrm{isld}}/w_{\mathrm{ion}}$ for $\omega = \omega_{*i}$ (blue triangles) and for $\omega = \omega_{*e}$ (red squares).

is approximated by $n_i \approx n_0 \left(1 - e\Phi/T_i\right)$. Since the small islands which we study are always big compared to the electron banana orbit width, we can take the solution for the electron distribution function for big islands. The leading terms which determine the density are [9]

$$f_e = f_{eM} \left\{ 1 + \frac{e\Phi}{T_e} - \frac{e}{T_e} \frac{q(\omega - \omega_{*e})}{m} \left(\psi - \psi_s + h\right) \right\}, \tag{24}$$

where $h(\Omega)$ denotes the Ω-dependent part (i. e. the second term) on the right-hand side of equation (8). Equating the resulting density with the ion density leads to

$$\Phi_{\mathrm{small}} \approx \frac{T_i}{T_i + T_e} \frac{q(\omega - \omega_{*e})}{m} \left(\psi - \psi_s + h\right) \tag{25a}$$

$$= \frac{T_i}{T_i + T_e} \left(1 - \frac{\omega_{*e}}{\omega}\right) \Phi_{\mathrm{big}} \tag{25b}$$

$$= \frac{T_i + T_e \left(\omega_{*i}/\omega\right)}{T_e + T_i} \Phi_{\mathrm{big}} \tag{25c}$$

with the potential Φ_{big} given in equation (8). At frequencies near the ion diamagnetic frequency the potential in small islands is about the same as that in big islands, while it is very small for frequencies near the electron diamagnetic frequency. In Fig. 10 results of simulations with this modified electric potential are shown, and the dependence of the island bootstrap current on the rotation frequency is depicted in Fig. 11. In the case $\omega = \omega_{*e}$ with a vanishing electric potential the density remains unperturbed, the mismatch of the electron
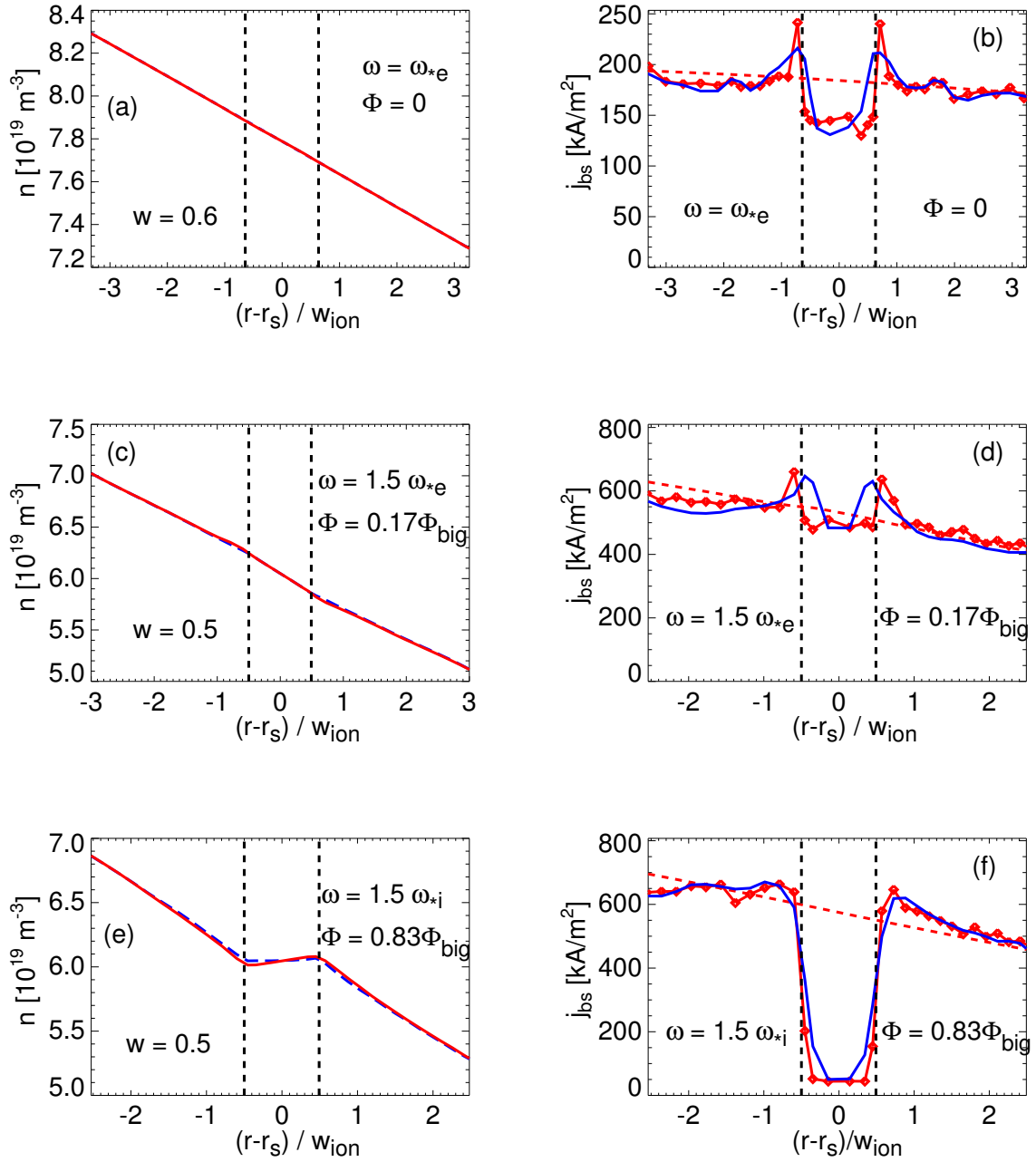
17

FIG. 10: Results from simulations with the modified electric potential in equation (25a): (a,c,e) electron density (red solid) and ion density (blue dashed) profiles, (b,d,f) bootstrap current from simulations (red symbols), neoclassical value computed with the perturbed gradients (solid blue line) and the unperturbed current (oblique dashed line). Vertical dashed lines indicate the position of the island.
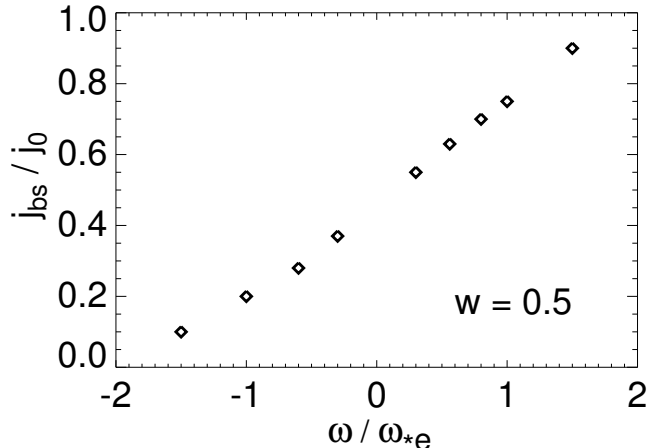
18

FIG. 11: Bootstrap current in a small island ($w = 0.5$) normalized to the unperturbed current versus island rotation frequency. Data from simulations with modified electric potential.

and ion densities is removed. The temperature profiles are not different from those in Sec. IV A, hence there is some reduction of the bootstrap current in the island caused by the flattening of the electron temperature. Inspite of the flattening of the electron temperature the current in the island rotating at $\omega = 1.5\,\omega_{*e}$ is almost equal to the unperturbed current, because the density is steepened inside the island. In the case $\omega = 1.5\,\omega_{*i}$ the current in the island is very small. This confirms the result from Sec. IV A that the most of the bootstrap current in the island is lost for $\omega \approx \omega_{*i}$, but that a large fraction is preserved for $\omega \approx \omega_{*e}$.

V. SUMMARY

The bootstrap current in rotating islands that are of similar size or smaller than the ion banana orbit width has been computed with drift kinetic numerical simulations. A frame of reference is used in which the unperturbed electric field vanishes. When the island is rotating in this frame, there is a radial electric field E_r that leads to an additional contribution to the parallel flows of ion and electrons of magnitude $u_\parallel \sim E_r/B_p$, where B_p is the poloidal component of the magnetic field. Since the electric field varies on the scale of the island width, which is much larger than the typical electron-orbit size, but comparable to the ion orbit width, the electrons react to the local field while the ions respond rather to the orbit-averaged field. The resulting parallel electron and ion flows differ from each other,

19

thus contributing to the parallel (bootstrap) current. The electric field also causes a density perturbation such that this current can be explained as the bootstrap current caused by this perturbation.

We have shown that when the island is rotating at a frequency near the ion diamagnetic frequency, most of the bootstrap current is lost even in small islands, only the contribution due to the ion temperature gradient remains present. In the case of rotation at a frequency near the electron diamagnetic frequency a large part of the bootstrap current is preserved in the island, and only the contribution due to the electron temperature gradient is lost. In this case the electric potential differs strongly from that in big islands. In all cases the bootstrap current is close to the value of the neoclassical theory computed with the perturbed density and temperature gradients.

Since the parallel current in the island influences the island dynamics, our results have a particular relevance for the prediction of the stability of magnetic islands. In small islands rotating in the ion diamagnetic direction, the bootstrap current drive of the island growth is strong like in big islands, since most of the bootstrap current is lost also in these small islands. However, in small islands rotating in the electron diamagnetic direction are more stable, since the bootstrap current is largely preserved by the "small-island effect" presented in this paper, hence the neoclassical drive of the island growth is strongly reduced. The competition between this effect and other (de)stabilizing effects acting on small islands (like e. g. finite transport across the island [4] or the polarization current [8, 9, 18]) is likely to explain the experimental finding that magnetic islands often appear only above a given amplitude threshold, implying some stabilising effect acting against the neoclassical drive for small islands.

[1] O. Sauter, R. J. La Haye, Z. Chang *et al.*, Phys. Plasmas **4**, 1654 (1997)

[2] W. X. Qu and J. D. Callen, University of Wisconsin Plasma Report No. UWPR 85-5, 1985.

[3] R. Carrera, R. D. Hazeltine and M. Kotschenreuther, Phys. Fluids **29**, 899 (1986).

[4] R. Fitzpatrick, Phys. Plasmas **2**, 825 (1995).

[5] E. Poli, A. G. Peeters, A. Bergmann *et al.*, Phys. Rev. Lett. **88**, 075001 (2002).

[6] E. Poli, A. G. Peeters, A. Bergmann *et al.*, Plasma Phys. Contr. Fusion **45**, 71 (2003).

[7] F. Hinton and R. Hazeltine, Rev. Mod. Phys. **48**, 239 (1976).

[8] A. I. Smolyakov, Plasma Phys. Controlled Fusion **35**, 657 (1993).

[9] H. R. Wilson, J. W. Connor, R. J. Hastie and C. C. Hegna, Phys. Plasmas **3**, 248 (1996).

[10] A. Bergmann, E. Strumberger and A. G. Peeters, Nucl. Fusion **45**, 1255 (2005).

[11] S. D. Pinches, L. C. Appel, J. Candy *et al.*, Comput. Phys. Commun. **111**, 133 (1998).

[12] A. Bergmann, A. G. Peeters and S. D. Pinches, Phys. Plasmas **8**, 5192 (2001).

[13] S. J. Allfrey and R. Hatzky, Comput. Phys. Commun. **154**, 98 (2003).

[14] A. M. Dimits and B. I. Cohen, Phys. Rev. E **49**, 709 (1994).

[15] Z. Lin, W. M. Tang, W. W. Lee, Phys. of Plasmas **2**, 2975 (1995).

[16] E. Poli, A. Bergmann, A. G. Peeters *et al.*, Nucl. Fusion **45**, 384 (2005).

[17] S. P. Hirshman and D. J. Sigmar, Nucl. Fusion **21**, 1079 (1981); O. Sauter, C. Angioni and Y. R. Lin-Liu, Phys. Plasmas **6**, 2834 (1999).

[18] A. B. Mikhailovskii, Contrib. to Plasma Phys. **43**, 125 (2003).

[19] F. L. Waelbroeck, J. W. Connor and H. R. Wilson, Phys. Rev. Lett. **87**, 215003 (2001).